1-1-2015

Facile method to synthesize Na-enriched Na1+xFeFe(CN)6 frameworks as cathode with superior electrochemical performance for sodium-ion batteries

Weijie Li
University of Wollongong, wl347@uowmail.edu.au

Shulei Chou
University of Wollongong, shulei@uow.edu.au

Jiazhao Wang
University of Wollongong, jiazhao@uow.edu.au

Yong-Mook Kang
Kongju National University, Dongguk University

Jianli Wang
University of Wollongong, jianli@uow.edu.au

See next page for additional authors

Facile method to synthesize Na-enriched Na1+xFeFe(CN)6 frameworks as cathode with superior electrochemical performance for sodium-ion batteries

Abstract

Different Na-enriched $Na_{1+x}FeFe(CN)_6$ samples can be synthesized by a facile one-step method, utilizing $Na_4Fe(CN)_6$ as the precursor in a different concentration of NaCl solution. As-prepared samples were characterized by a combination of synchrotron X-ray powder diffraction (S-XRD), Mössbauer spectroscopy, Raman spectroscopy, magnetic measurements, thermogravimetric analysis, X-ray photoelectron spectroscopy, and inductively coupled plasma analysis. The electrochemical results show that the $Na_{1.56}Fe[Fe(CN)_6]\cdot 3.1H_2O$ (PB-5) sample shows a high specific capacity of more than 100 mAh g^{-1} and excellent capacity retention of 97% over 400 cycles. The details structural evolution during Na-ion insertion/extraction processes were also investigated via *in situ* synchrotron XRD. Phase transition can be observed during the initial charge and discharge process. The simple synthesis method, superior cycling stability, and cost-effectiveness make the Na-enriched $Na_{1+x}Fe[Fe(CN)_6]$ a promising cathode for sodium-ion batteries.

Keywords

method, batteries, facile, cathode, sodium, electrochemical, superior, frameworks, 6, cn, xfefe, na1, enriched, na, synthesize, ion, performance

Disciplines

Engineering | Physical Sciences and Mathematics

Publication Details

Li, W., Chou, S., Wang, J., Kang, Y., Wang, J., Liu, Y., Gu, Q., Liu, H. & Dou, S. (2015). Facile method to synthesize Na-enriched $Na_{1+x}FeFe(CN)_6$ frameworks as cathode with superior electrochemical performance for sodium-ion batteries. Chemistry of Materials, 27 (6), 1997-2003.

Authors

Weijie Li, Shulei Chou, Jiazhao Wang, Yong-Mook Kang, Jianli Wang, Yong Liu, Qinfen Gu, Hua-Kun Liu, and S X. Dou

2015

A facile method to synthesize Na-enriched $Na_{1+x}FeFe(CN)_6$ frameworks as cathode with superior electrochemical performance for sodium-ion batteries

Wei-Jie Li,[1] Shu-Lei Chou,[1,] Jia-Zhao Wang,[1] Yong-Mook Kang,[2] Jian-Li Wang,[1] Yong Liu,[3] Qin-Fen Gu,[4] Hua-Kun Liu,[1] Shi-Xue Dou[1]*

1Institute for Superconducting and Electronic Materials, University of Wollongong, Wollongong, NSW 2522 Australia

E-mail: shulei@uow.edu.au

2 Department of Energy and Materials Engineering, Dongguk University-Seoul, Seoul, 100-715, Republic of Korea

3Institute of Advanced Materials for Nano-Bio Applications, School of Ophthalmology & Optometry, Wenzhou Medical University, Wenzhou, Zhejiang 325027, China.

4Australian Synchrotron, 800 Blackburn Rd, Clayton 3168, Australia

.

KEYWORDS: Na-enriched $Na_{1+x}FeFe(CN)_6$, high specific capacity, superior long cycle-life, sodium ion batteries

ABSTRACT: Different Na-enriched $Na_{1+x}FeFe(CN)_6$ samples can be synthesized by a facile one-step method, utilizing $Na_4Fe(CN)_6$ as the precursor in a different concentration of NaCl solution. As-prepared samples were characterized by a combination of synchrotron X-ray powder diffraction (S-XRD), Mössbauer spectroscopy, Raman spectroscopy, magnetic measurements, thermogravimetric analysis, X-ray photoelectron spectroscopy, and inductively coupled plasma analysis. The electrochemical results show that $Na_{1.56}Fe[Fe(CN)_6]\cdot 3.1H_2O$ (PB-5) sample shows a high specific capacity of more than 100 mAh g^{-1} and excellent capacity retention of 97% over 400 cycles. The details structural evolution during Na-ion insertion/extraction processes were also investigated via *in-situ* synchrotron XRD. Phase transition can be observed during the initial charge and discharge process. The simple synthesis method, superior cycling stability, and cost-effectiveness make the Na-enriched $Na_{1+x}Fe[Fe(CN)_6]$ a promising cathode for sodium-ion batteries.

Renewable energy sources, such as wind and sun, have attracted ever-growing attention due to exhaustion of fossil fuels and environmental concerns. Due to the intermittent nature of the renewable energy the utilization of these energy sources relies on the availability of large-scale energy storage systems (ESS).[1] In cases, lithium ion batteries (LIBs) are not suitable candidates because of the low abundance of lithium resources and high cost. In comparison, sodium is abundant and cheap, and also has similar physical and chemical properties to Lithium. Thus, more and more investigations on sodium ion batteries (SIBs) have been emerging in recent

years.[2-3]

In a full cell, the cathode material determines the final charge-discharge capacity. Hence, it is crucial to develop a non-toxic, low-cost, high-capacity, stable cathode material for SIBs to ensure large-scale and long-term applications. Up to now, transition metal (M) oxides (Na_xMO_{2+y}),[4-8] phosphates,[9-12] fluorides,[13] and hexacyanoferrates[14-17] have been reported as cathode materials for SIBs. Few materials, however, can have both high capacity (> 100 mAh g-1) and long cycle life simultaneously. Among these materials, iron hexacyanoferrate is a promising cathode material due to its low cost and non-toxicity. Yang's group reported that $FeFe(CN)_6$ had good cycling stability with a slight capacity decay from the initial 120 to 115 mAh g^{-1} after 150 cycles,[18] and Goodenough's group also suggested that $KFeFe(CN)_6$ exhibits excellent capacity retention of more than 99% after 30 cycles.[15] A fatal flaw, however, is that $FeFe(CN)_6$ and $KFeFe(CN)_6$ do not have sodium ions, which hinders their application in sodium ion batteries. Qian et al. ball milled $Na_4Fe(CN)_6$ with super P to obtain a $Na_4Fe(CN)_6$/C composite which displayed superior cycling stability, with a 88% capacity retention over 500 cycles at a current density of 9 mA g^{-1}, but its theoretical discharge capacity was only 87 mAh g^{-1} because it had just one redox site.[19] Yu et al. demonstrated that $NaFeFe(CN)_6$ can deliver a capacity as high as 118 mAh g^{-1} at 5 mA g^{-1} current density, however, after 20 cycles, the capacity retention was 85% of that in the 2nd cycle.[20] If we can prepare a material which combines the high capacity of $NaFeFe(CN)_6$ with the excellent cycling stability of $Na_4Fe(CN)_6$, it will represent a big improvement in the energy storage field.

Prussian blue (PB) has the perovskite-type structure, $A_2M^{II}[T^{II}(CN)_6]$ (A: alkali metal; M and T: transition metal), in which there are two redox reaction metals. Thus, the ideal electrochemical reaction is $A_2M^{II}[T^{II}(CN)_6] \leftrightarrow 2A^+ + 2e^- + M^{III}[T^{III}(CN)_6]$, which can achieve maximum ion storage ($2A^+$). The synthetic procedure for PB is in aqueous solution, however, so

the general formula of PB as it is prepared is $A_xM[T(CN)_6]_{1-y}\square_y\, nH_2O$ ($0 < x < 2$, $y < 1$), where □ denotes a $[T(CN)_6]$ vacancy occupied by coordinating water.[21] The presence of vacancies and coordinating water will break down the bridging of the M-CN-T framework, resulting in a distorted lattice, which gives rise to lower efficiency and structural instability of the PB compound during the charge-discharge process.[18] Therefore, it is important to fabricate a PB framework with few vacancies. Recently, Guo's group reported that $Na_{0.61}Fe[Fe(CN)_6]_{0.94}\cdot\square_{0.06}$ with few vacancies had been prepared by a facile method and could be stably cycled over 150 cycles without apparent capacity loss.[22] There is a serious problem for this reported material, however, that the content of Na-ions per molecular formula unit is very low, and as a result, it must be initially discharged, which is not applicable for the sodium-ion full cell.

Here, we report Na-enriched $Na_{1+x}FeFe(CN)_6$ synthesized by a facile one-step method, utilizing $Na_4Fe(CN)_6$ as the precursor in a saturated NaCl solution. In this method, more sodium ions enter into the framework, which not only can effectively reduce the amount of vacancies and coordinating water, but also can increase the amount of sodium ions per formula unit. As a result, this not only can enhance the cycling stability and the efficiency due to the reduction in the amount of vacancies and crystal water, but also can improve the specific capacity, due to the benefit from more sodium ions entering into the framework.

RESULTS AND DISCUSSION

To introduce more Na^+ into the framework, a series of $Na_{1+x}Fe[Fe(CN)_6]$ samples were prepared in different concentrations of NaCl solutions. The samples prepared in 0 M, 0.34 M, 1.2 M, 3.6 M, and 6.16 M NaCl solutions, are denoted as PB-1, PB-2, PB-3, PB-4, and PB-5, respectively. The lab X-ray powder diffraction (XRD) patterns of all samples show distinguish peaks, indicating that all synthesized samples are well crystallized phase (Figure S1 in the

Supporting Information). All main peaks can be indexed to a cubic (space group F*m-3m*) unit cell, which is close to reported pristine $Na_{1+x}Fe[Fe(CN)_6]$ structure in ICDD PDF-4 database (2014). With higher concentrations of NaCl solutions added in, the XRD patterns show a trend of peaks shift to smaller 2 theta angles. For example, the pristine $Na_{1+x}Fe[Fe(CN)_6]$ prepared without the addition of NaCl showed a (200) peak at 2θ about 17.46°. When 2 g NaCl was added into the solution (0.34 M), the (200) peak shifted to smaller angle, about 17.28°. Further increasing the amount of NaCl, the XRD peaks gradually shifted to even smaller diffraction angles, down to about 17.14° for PB-5 prepared in saturated NaCl solution, indicating that the spaces of the lattice planes had increased. Also, the energy dispersive spectroscopy (EDS) results show that the sodium content increased from 3.172 at% for PB-1 to 6.683 at% for PB-5 (Table S1, Supporting Information). It is suggested that the increased concentration of sodium ions in the precursor solution resulted for more Na^+ ions entry into the unit cell enlarged the interplanar distance, and increased lattice parameters of the PB phases. Scanning electron microscope (SEM) images show that $Na_{1+x}Fe[Fe(CN)_6]$ compound has a cubic morphology, and its particle size is about 0.5-3 μm, which is favourable for the improvement of tap density (Figure S2). It should be noted that the average particle size of $Na_{1+x}Fe[Fe(CN)_6]$ decreased with higher concentrations of sodium ions in the precursor solution (Supporting Information, Figure S2). This result is also consistent with refined S-XRD data of crystalline size of 3696nm, 1097nm, 832nm for PB-1, PB-3, and PB-5, respectively. PB-1, PB-3, and PB-5 were selected as the main samples to investigate the structural evolution of the PB framework after more sodium was introduced into the framework.

In order to further explore the structural evolution of the different $Na_{1+x}Fe[Fe(CN)_6]$ samples, synchrotron X-ray powder diffraction (S-XRD) experiment was conducted at room temperature

on the Powder Diffraction Beamline at the Australian Synchrotron. The S-XRD data for PB-1, PB-3, and PB-5 were refined with GSASΠ software,[23] and the Rietveld refinement results are plotted in Figure 1(a). The changes in the crystal lattice caused by the introduction of more sodium ions into the PB framework can be clearly seen that the lattice parameter *a* increased from 10.3028 Å for PB-1, 10.3122(1) Å for PB-3 to 10.3304(1) Å for PB-5 sample, with 0.268% increased (Figure 1(b). This demonstrates that more sodium ions could enter into the framework in PB-5, resulting in the expansion of crystal lattice of the $Na_{1+x}Fe[Fe(CN)_6]$ framework. The crystal structure of the $Na_{1+x}Fe[Fe(CN)_6]$ is shown in inset of Figure 1(b). Na atoms locate at *8c* position in the structure. Each Na atom is in the middle of void, which surrounded by eight Fe atoms forming a cubic lattice. The Na-Fe distance increased from 4.461 Å to 4.473 Å, in PB-1 to PB-5 phases. The occupation of the atoms in the $Na_{1+x}Fe[Fe(CN)_6]$ framework based on the refinement is listed in Table S2 (Supporting Information). Significantly, there were more sodium ions in the PB-5 framework by comparison with PB-1 and PB-3. Meanwhile, the amount of C≡N groups in the PB-5 framework increased, suggesting that the amount of vacancies decreased from PB-1 to PB-5. Moreover, the amount of O atoms, which come from the crystalline water, decreased gradually from the PB-1 to the PB-5 sample, demonstrating that the coordinating water in the crystal decreased with more sodium-ion occupation in the PB framework. Consequently, the structure of PB-5 sample forms one framework that is Na-enriched and has few vacancies, and it was synthesized by a facile one-step method, just utilizing $Na_4Fe(CN)_6$ as the precursor in a saturated NaCl solution. This method not only can effectively reduce the amount of vacancies and coordinating water, but also can increase the amount of sodium ions per formula unit.

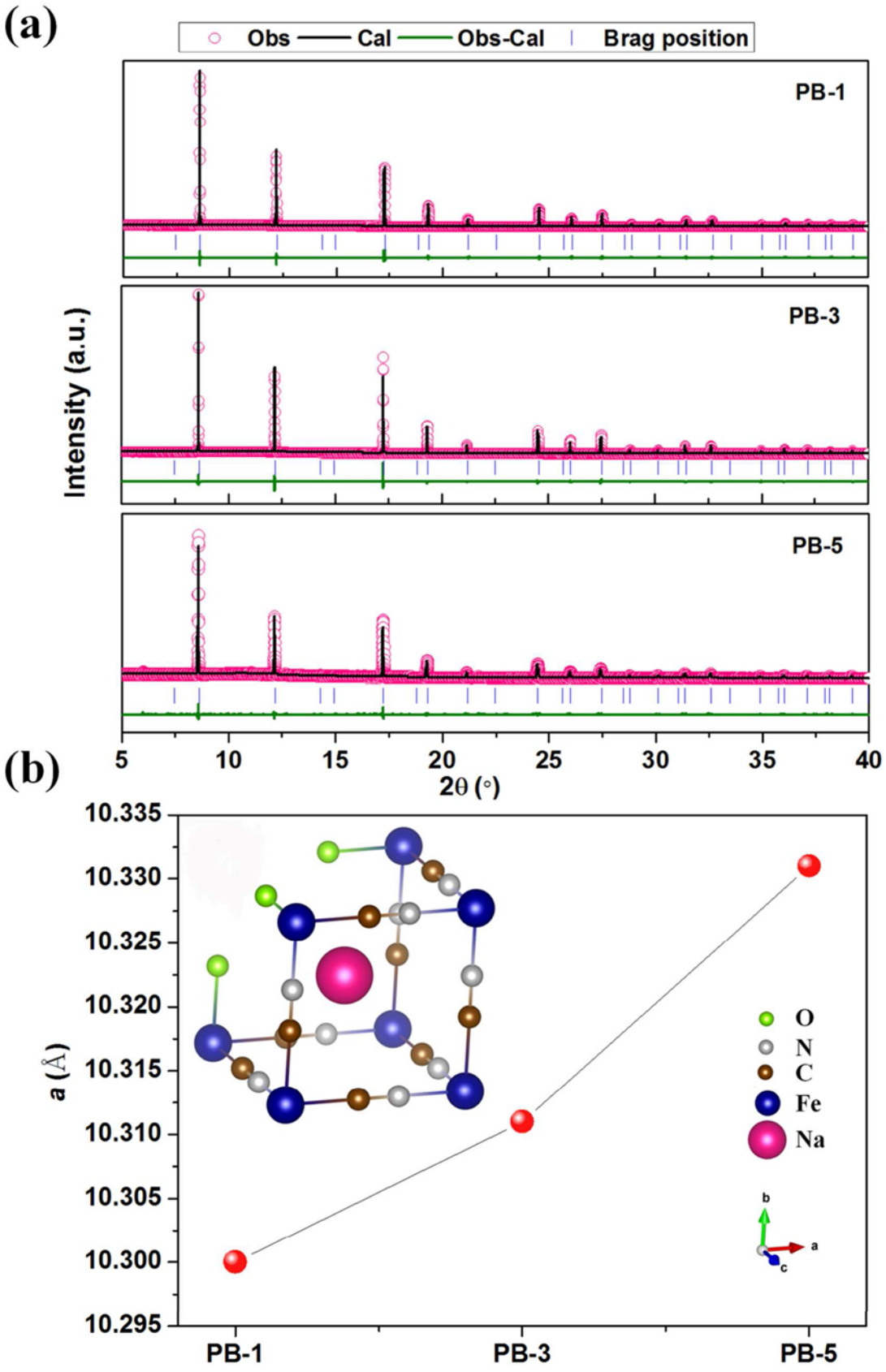
(a)
Obs
Cal
Obs-Cal
Brag position
PB-1
PB-3
PB-5
Intensity (a.u.)
5
10
15
20
25
30
35
40
2θ (°)
(b)
10.335
10.330
10.325
10.320
10.315
10.310
10.305
10.300
10.295
a (Å)
PB-1
PB-3
PB-5
O
N
C
Fe
Na
b
a
c

Figure 1. (a) Synchrotron XRD patterns of PB-1, PB-3, and PB-5, and their Rietveld refinements. (b) Lattice parameters changes of the $Na_{1+x}Fe[Fe(CN)_6]$ powders and the crystal structure of the $Na_{1+x}Fe[Fe(CN)_6]$ framework based on the S-XRD refinement inset. (The synchrotron X-ray powder diffraction was obtained from the Powder Diffraction Beamline at the Australian Synchrotron, with wavelength of 0.7747 Å.)

Figure 2(a) shows the Raman spectra of the $Na_{1+x}Fe[Fe(CN)_6]$ powders between 2000 and 2300 cm^{-1}. Three peaks at 2083.8, 2122.0 and 2139.4 cm^{-1} were observed from PB-1, PB-3 and PB-5. All these peaks can be assigned to the $(C\equiv N)^-$ group, reflecting the bonding of the $(C\equiv N)^-$ ion to the Fe ions in different valence states. The higher is the iron oxidation state, the more effective is the iron cation to $(C\equiv N)^-$ bonding. [24-25] Thus, the peak at 2139.4 cm^{-1} is assigned to the bonding of the $(C\equiv N)^-$ to Fe^{3+} ion. Clearly, with more sodium ion entry into the framework, the intensity of the peak at 2139.4 cm^{-1} decreased gradually, suggesting the amount of Fe^{3+} in the $Na_{1+x}Fe[Fe(CN)_6]$ decreased. Thermogravimetric analysis (TGA) was carried out in argon from 50 to 600 $^{\circ}C$ at a heating rate of 10 $^{\circ}C$/min, to determine the water content in the $Na_{1+x}Fe[Fe(CN)_6]$ powders, as shown in Figure 2(b). It is clear that there is a considerable amount of water in the prepared compounds. A trace amount of water (lost at ~ 100 $^{\circ}C$) was adsorbed on the particle surfaces, while much water was adsorbed in the vacancies (evaporating in the range of 200 – 350 $^{\circ}C$). The water content of PB-1, PB-3, and PB-5 was 18.7, 17.2, and 15.5 wt %, respectively. The TGA results confirm that the introduction of more Na^+ into the $Na_{1+x}Fe[Fe(CN)_6]$ framework reduces the amount of crystal water in the unit cell. The molar Na : Fe ratios of the PB samples were detected by inductively coupled plasma (ICP). The molar ratios were calculated to be 0.633, 0.663, and 0.778 for PB-1, PB-3, and PB-5, respectively. Combined

with the TGA results, the formulas for PB-1, PB-3, and PB-5 are $Na_{1.26}Fe[Fe(CN)_6]\cdot 3.8H_2O$, $Na_{1.33}Fe[Fe(CN)_6]\cdot 3.5H_2O$ and $Na_{1.56}Fe[Fe(CN)_6]\cdot 3.1H_2O$, respectively.

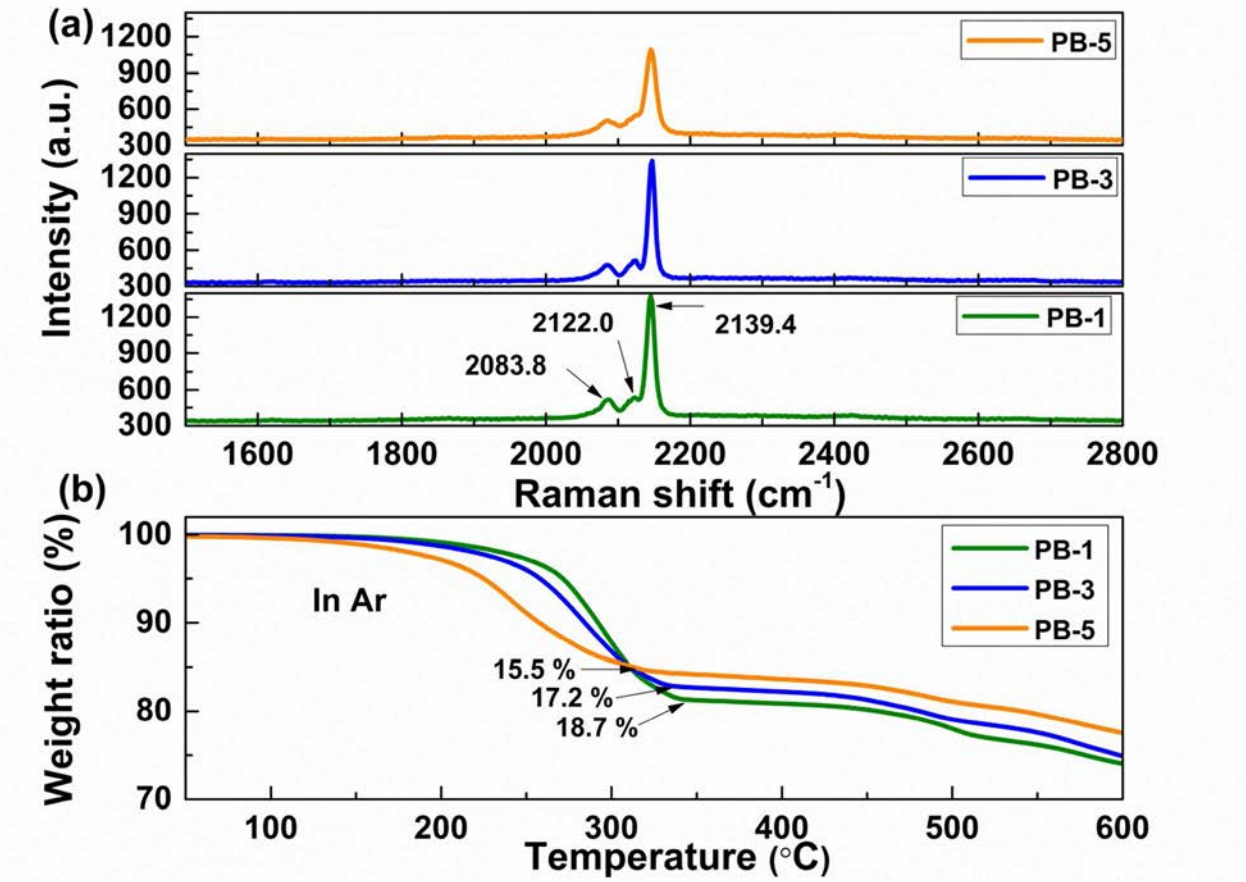

Figure 2. (a) Raman spectra and (b) TGA analysis of $Na_{1+x}Fe[Fe(CN)_6]$ powder samples.

In order to further determine the spin state of Fe in the as-prepared samples, Mössbauer spectroscopy was performed, and the results are shown in Figure 3. From the Mössbauer spectroscopy results, it is clearly seen that the $Na_{1+x}Fe[Fe(CN)_6]$ powder contains Fe^{2+} and Fe^{3+} ions. (The occupancy of Fe^{2+} and Fe^{3+} are listed in Table S3.) In the PB-1 sample, 82.7 % of the Fe was in the Fe^{3+} state. With increased sodium content in the $Na_{1+x}Fe[Fe(CN)_6]$, the amount of Fe^{3+} decreased, down to 62.1 % for PB-5, while the percentage of Fe^{2+} changed in the opposite way, increasing from 17.3 % for PB-1 to 37.9 % for PB-5. This trend is consistent with the Raman Spectra (Figure 2) and the X-ray photoelectron spectroscopy (XPS) results (Figure S3).

Moreover, the decrease in Fe^{3+}, accompanied by the increase in Fe^{2+}, suggested that $[Fe(CN)_6]$ vacancy exists in the unit cell, and the formula of the as-prepared PB is $Na_{1+x}Fe^{III}[Fe^{II}(CN)_6]_{1-y}\square_y \cdot nH_2O$ ($0 < x < 1$, $y < 1$). Otherwise, the ratio of Fe^{2+} to Fe^{3+} should remain 1:1. In other words, with more sodium ion entering into the crystal structure, the ratio of Fe^{2+} to Fe^{3+} becomes closer to 1 (41.8 % : 58.2 % = 0.718), suggesting that amount of $[Fe(CN)_6]$ vacancy becomes less at the same time, while the amount of coordinating water occupying the vacancy becomes less (as seen from the TGA results in Figure 2(b)), which indicates the better ordering in the lattice. Thus, it is concluded that PB prepared in saturated NaCl solution have an increased content of sodium and reduced amounts of vacancy and coordinating water in the formula for Prussian blue. This is beneficial for the improvement of both the capacity and the structural stability of the PB compound during charge-discharge processes.

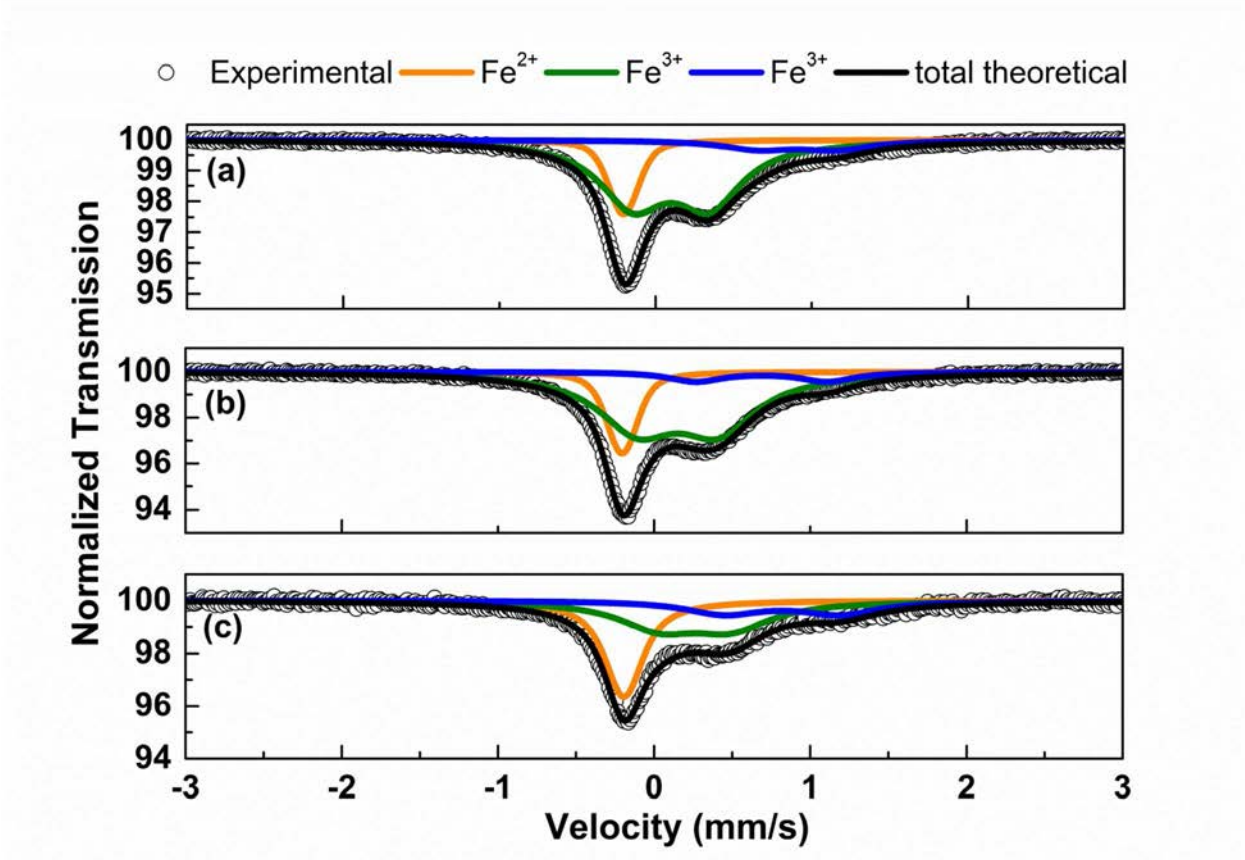

Figure 3. Mössbauer spectra of (a) PB-1, (b) PB-3, and (c) PB-5 samples.

To promote electron beam penetration into the particles, the micro sized $Na_{1+x}Fe[Fe(CN)_6]$ samples (~2 μm) were crushed into small pieces in a mortar before working on transmission electron microscopy (TEM). The selected area electron diffraction (SAED) patterns show that the $Na_{1+x}Fe[Fe(CN)_6]$ particles were single crystalline with face-centred-cubic structure (insets of Figure 4). It is difficult, however, to observe the lattice fringes in high resolution TEM (HRTEM) of $Na_{1+x}Fe[Fe(CN)_6]$ particles because the unstable structure will be changed under higher voltage (Figure 4).

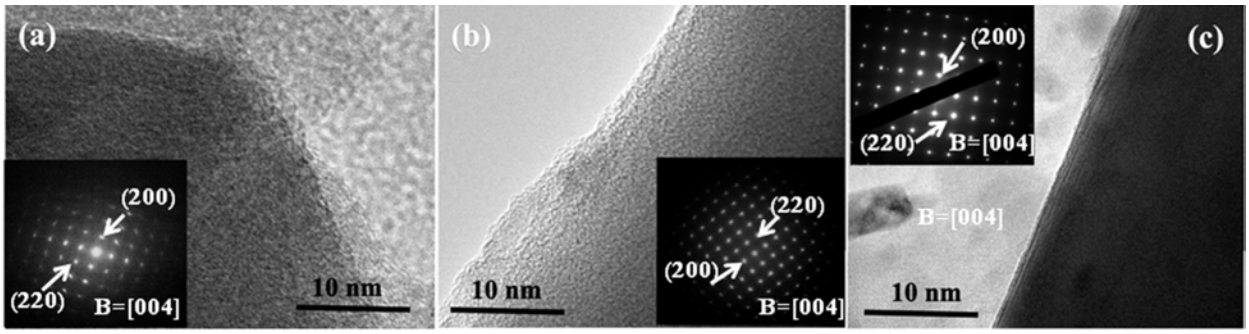

Figure 4. TEM images and SAED patterns (insets) of (a) PB-1, (b) PB-3, and (c) PB-5.

Figure 5(a) shows the charge-discharge curves of $Na_{1+x}Fe[Fe(CN)_6]$ powders between 2.0 - 4.0 V at the current density of 20 mA g^{-1}. The PB-1 sample can deliver 86.5 mAh g^{-1} discharge capacity, but by comparison, the PB-3 and PB-5 samples can deliver larger capacity, 90.8 and 103.6 mAh g^{-1}, respectively. Moreover, the potential hysteresis (ΔE) between the charge and discharge curves is reduced for the PB-3 and PB-5 samples. There were two redox couples in the dQ/dV curve of PB-1 (Figure 5(b)), with the strong one located at 2.98/2.92 V and a small one at 3.74/3.42 V, which is similar to the cyclic voltammetry (CV) curves of $FeFe(CN)_6$.[18] It is likely that the different coordination sites of Fe ions in the $Na_{1+x}Fe[Fe(CN)_6]$ give rise to these two pairs of peaks in the dQ/dV curve. Thus, the peaks at 2.98/2.92 V are attributed to the high-spin

Fe^{II}/Fe^{III} couple coordinated with $(C\equiv N)^-$ by N atoms, and the ones at 3.74/3.42 V are assigned to the low-spin Fe^{II}/Fe^{III} couple bonding to the C atoms of the $(C\equiv N)^-$.[15] In the subsequent cycles, the shapes and areas of the dQ/dV curve in the 50th cycle overlapped well with the second cycle one, demonstrating the reversible and stable Na insertion/deinsertion reactions of the $Na_{1+x}Fe[Fe(CN)_6]$. Interestingly, for the PB-3 and PB-5 samples, an extra two pairs of peaks appeared in the dQ/dV curves at 3.06/3.04 V and 3.34/3.3 V, respectively (Figure 5(c, d)). This is the reason for the extra capacity of the PB-3 and PB-5 samples compared with the PB-1 sample, which is related to the spin states of Fe^{II} and Fe^{III}.

To identify the spin states of Fe^{II} and Fe^{III} in the $Na_{1+x}Fe[Fe(CN)_6]$, the dependence of the magnetic susceptibility (χ) of the $Na_{1+x}Fe[Fe(CN)_6]$ powders on temperature was obtained, as shown in Figure 6. All the $Na_{1+x}Fe[Fe(CN)_6]$ powders show paramagnetic behavior from low temperature, and there is no phase transition observed in this temperature range (Figure 6(a)). The calculated effective magnetic moments (μ_{eff}) of PB-1, PB-3, and PB-5 are 4.45 μ_B, 4.2 μ_B, and 4.0 μ_B per formula unit, respectively. Moreover, the effective magnetic moments for the low-spin (S = 1/2) and high-spin (S = 5/2) states of Fe^{III} are 1.73 and 5.9 μ_B, respectively, while those for the low-spin (S = 0) and high-spin (S = 2) states of Fe^{II} are 0 and 4.89 μ_B, respectively. In our present state of knowledge, it is just concluded from combining the calculated effective magnetic moments (μ_{eff}) with the dQ/dV curves that the Fe^{II} and Fe^{III} in the PB-3 and PB-5 have four different spin states. It is difficult to determine, however, what the two extra redox couples that appear in PB-3 and PB-5 samples should be assigned to.

2015

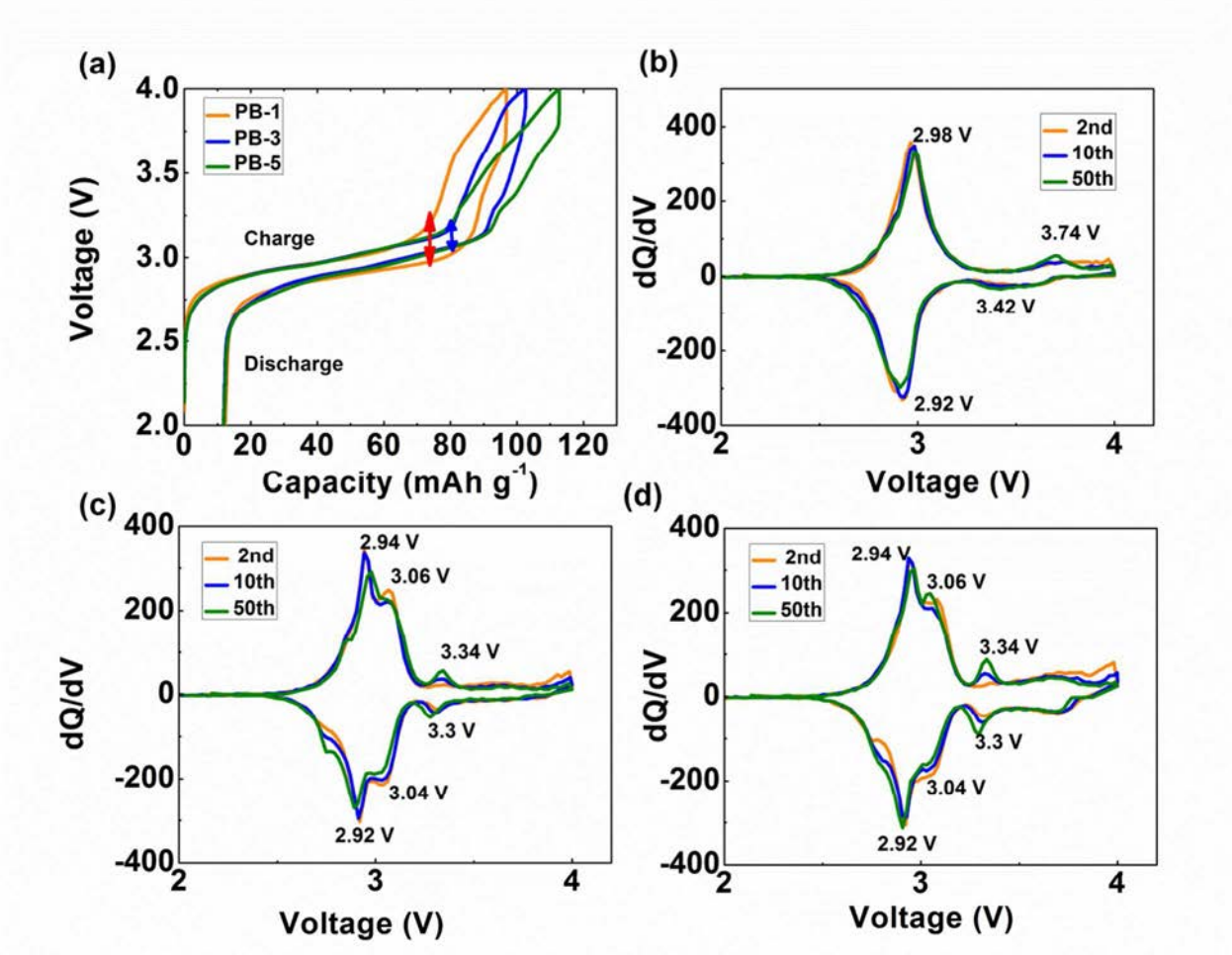

Figure 5 (a) Charge – discharge curves of $Na_{1+x}Fe[Fe(CN)_6]$ powders at current density of 20 mA g^{-1}; (b), (c), and (d) are dQ/dV curves of PB-1, PB-3, and PB-5, respectively.

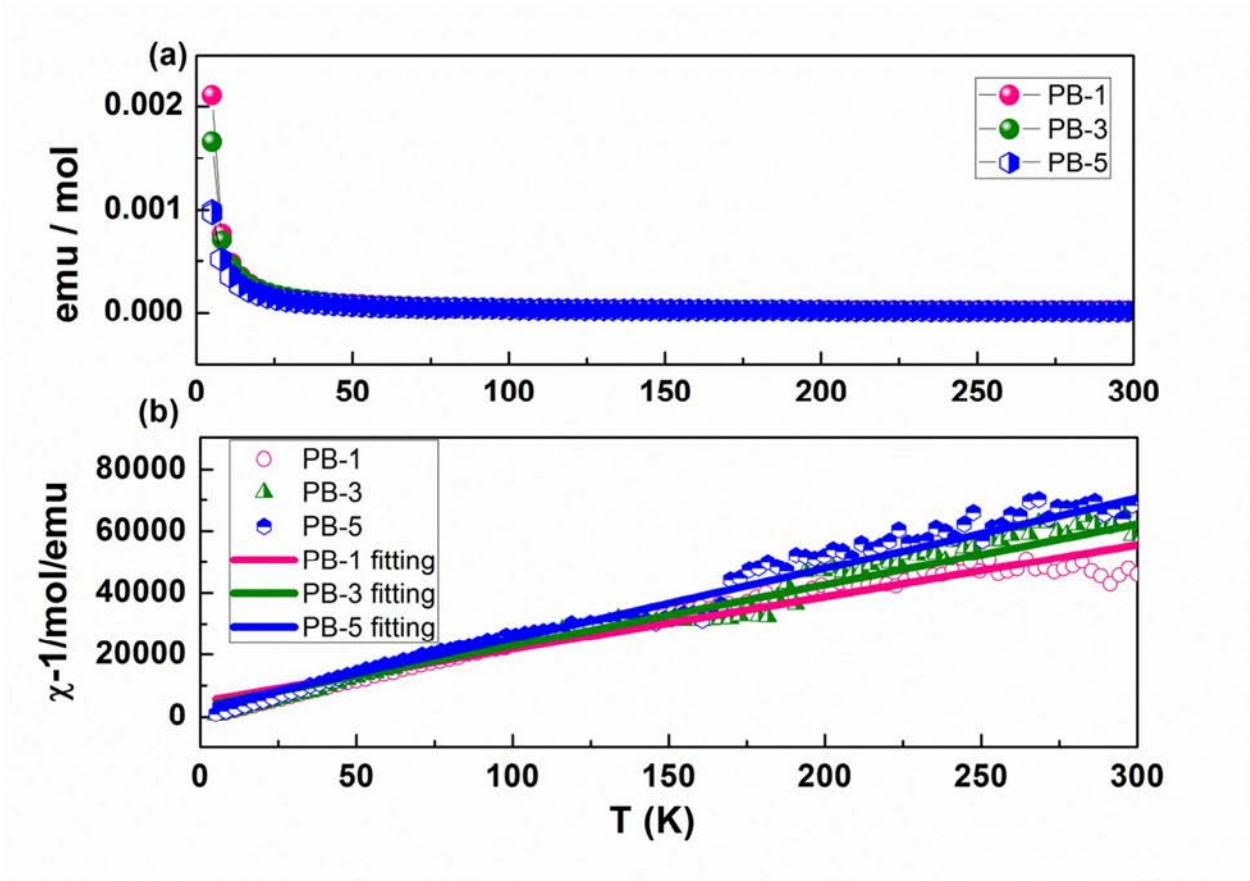

Figure 6. (a)Temperature dependence of the magnetic susceptibility of the $Na_{1+x}Fe[Fe(CN)_6]$ powders and (b) inverse susceptibilities corrected for the temperature-independent contribution and their fit to the Curie-Weiss law.

To investigate the structural evolution during Na-ion insertion/extraction processes, *in-situ* synchrotron pXRD was carried out on the Powder Diffraction Beam line at the Australian Synchrotron with a wavelength (λ) of 0.6888 Å. Figure 7 shows the *in-situ* pXRD patterns of the PB-5 cathode material during the first cycle within the voltage range of 2.0 - 4.0 V. From the image plots of the diffraction patterns for (200), (220), and (400), it is clear that the intensities of the (200) and (400) plane Bragg reflections decreased during charging, and the process was observed to be reversible during discharging (Figure 7(a)). The decrease/increase of the intensities during the charging/discharging suggests that the sodium ions were extracted from

and inserted into the structure of PB-5 reversibly. Additionally, the positions of the (200), (220), and (400) peaks shifted towards larger 2θ values during the charge process and could not be restored during the discharging process, indicating the contraction of the unit cell during sodium-ion insertion/extraction into the PB-5 framework. This decrease in the unit cell volume can explain why the discharge capacity of PB-5 is smaller than the capacity during the charge process. Moreover, some appreciable positive intensities within the 7.55° to 7.7° and 15.2° to 15.43° 2θ ranges indicate the existence of a phase with lattice parameters that deviate from those of PB-5 ($Na_{1.56}Fe[Fe(CN)_6]\cdot 3.1H_2O$). This phenomenon can be clearly observed in the close individual diffraction patterns of the (200) and (400) reflections stacked against the voltage profile (Figure 7(b)). At the onset of the charge, the peaks of the (200) and (400) reflections show symmetrical profiles, and then the reflections start to broaden asymmetrically toward higher angles. Finally, the peaks of the (200) and (400) reflections split into two peaks at the end of the charging process. The changes of lattice parameter *a* during the first cycle is plotted in Figure S4 (In Supporting Information). This is due to the phase transition that takes place from sodium-rich $Na_{1.56}Fe[Fe(CN)_6]\cdot 3.1H_2O$ ($Na_{1.56}$) to sodium-poor $Na_\delta Fe[Fe(CN)_6]\cdot nH_2O$ (Na_δ) during the charging process, which is also observed in $LiFePO_4$.[26] During the discharge process, with the sodium insertion into the framework, the peaks of the (200) and (400) reflections begin to narrow into symmetrical peaks and shift to smaller angle. Since the sodium composition cannot be restored to the original $Na_{1.56}Fe[Fe(CN)_6]\cdot 3.1H_2O$ at the end of the discharging process ($Na_{1.56-x}Fe[Fe(CN)_6]\cdot 3.1-yH_2O$ ($Na_{1.56-x}$)), the (200) and (400) peaks didn't shift back to their pristine positions. The valence state change of Fe in the PB-5 electrode during cycling was tested by the Mössbauer spectra, shown in Figure S5, which also support this point. When the PB-5 electrode was fully charged at 4.0 V, the percentage of Fe^{2+} decreased from 37.9% to 28.7%.

While the percentage of Fe^{2+} cannot restore to the original state, just 30.5% at the end of discharging process (Table S4). This also confirms that the sodium content of the PB-5 electrode at the end of the discharging process is lower than that of the original $Na_{1.56}Fe[Fe(CN)_6]\cdot 3.1H_2O$, in good agreement with the *in-situ* S-XRD observation. This irreversible structure change could also attribute to the removal of coordinating water in the Na-enriched phase.

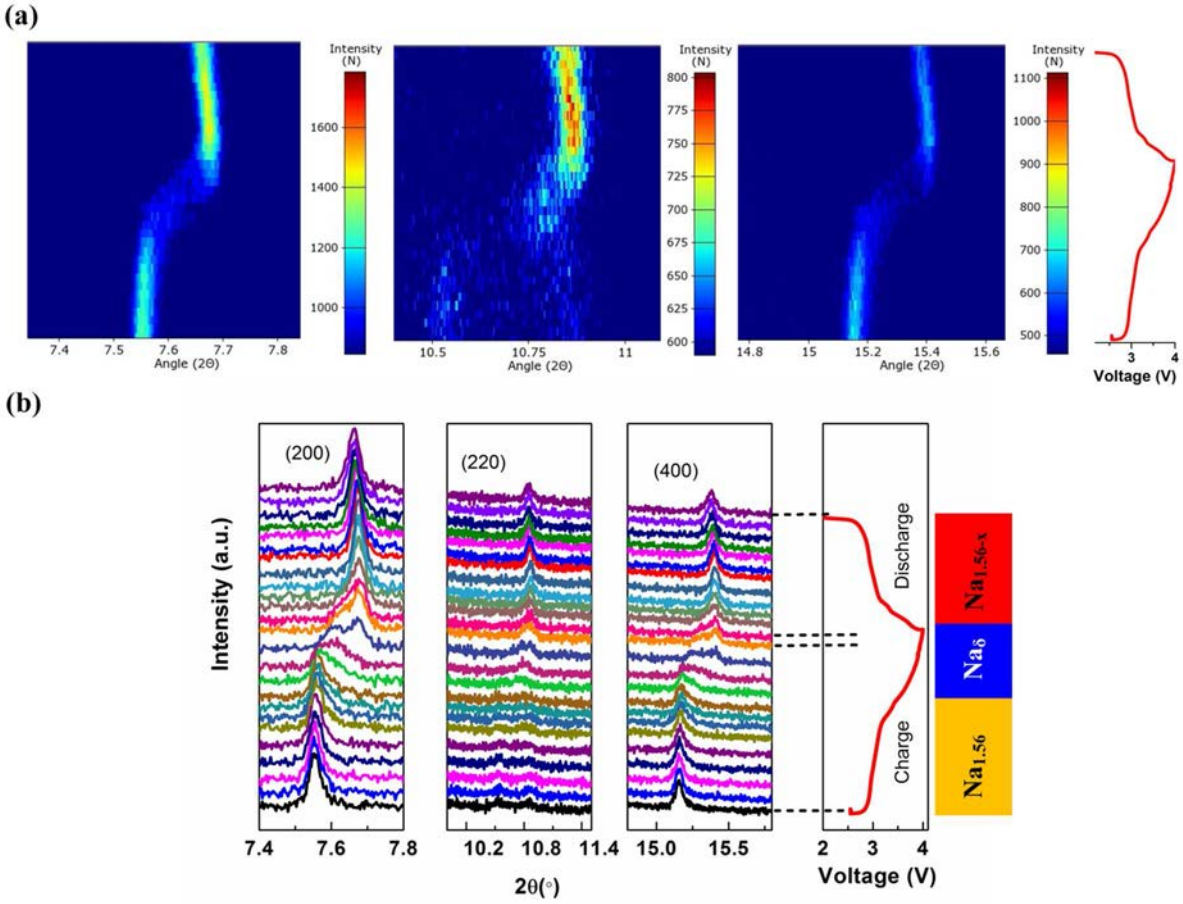

Figure 7. *In-situ* synchrotron pXRD patterns of PB-5 during the first charge and discharge at current density of 50 mA g^{-1}; (a) Image plots of diffraction patterns for the (200), (220), and (400) reflections during the first cycle. (b) Individual diffraction patterns of the (200), (220), and (400) reflections stacked against the voltage profile. (wavelength (λ) of 0.6888 Å, determined using the NIST LaB_6 660b standard reference material.)

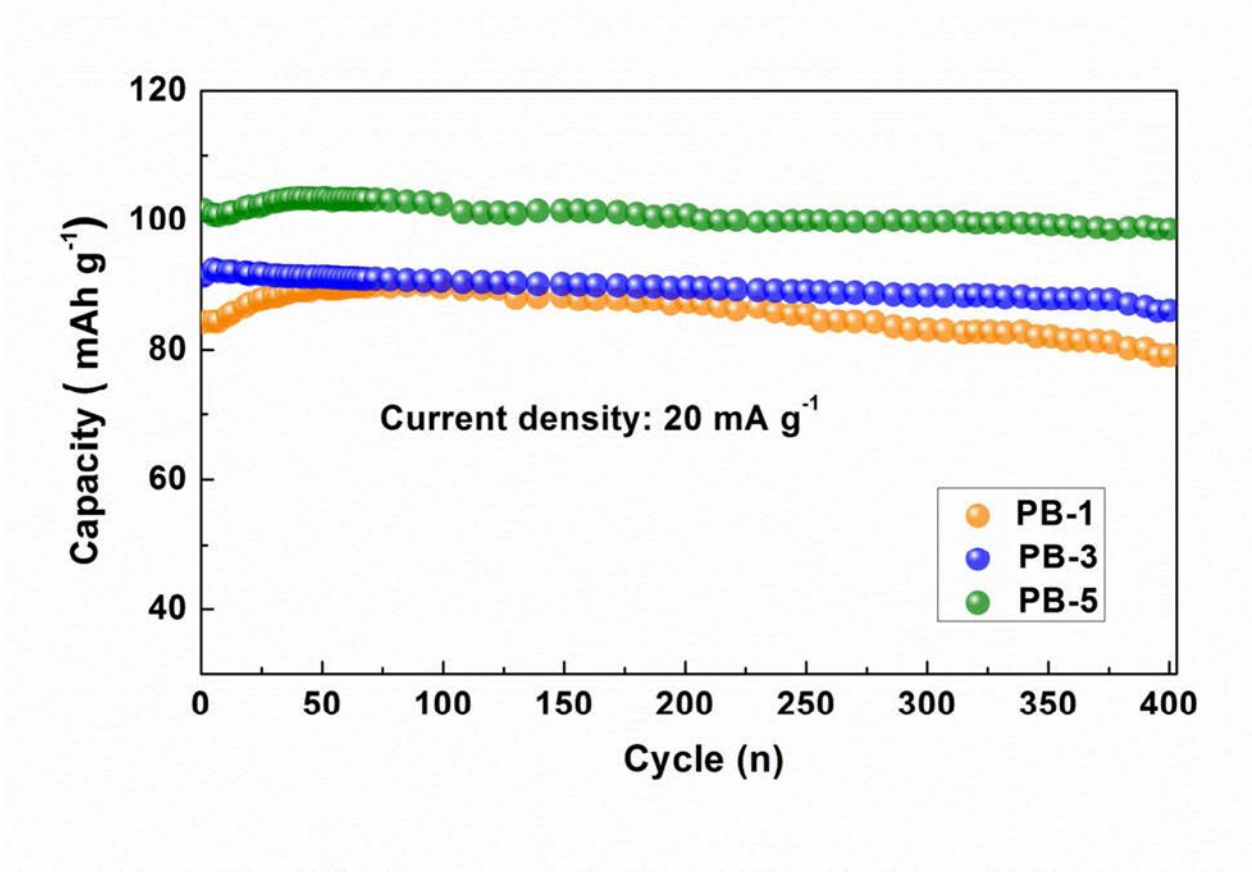

Figure 8. Cycling performance of $Na_{1+x}Fe[Fe(CN)_6]$ electrodes.

Figure 8 shows the cycling performance of the $Na_{1+x}Fe[Fe(CN)_6]$ cathodes between 4.0 - 2.0 V at the current density of 20 mA g^{-1}. It is clear that the cycling stability of the $Na_{1+x}Fe[Fe(CN)_6]$ is excellent; after 400 cycles, there was a slight capacity decay. The PB-5 sample, which had the most sodium ion content and the least vacancy in its framework, delivered a larger capacity of 103 mAh g^{-1}, compared with the PB-1 sample with capacity of 89.5 mAh g^{-1}. After 400 cycles, the capacity of PB-5 was still 97% of the initial capacity, while the capacity retention of PB-1 was 91%, which was also higher compared with other cathode materials for sodium-ion batteries.[4-17] This demonstrates that the reduction of the vacancies and coordinating water in the $Na_{1+x}Fe[Fe(CN)_6]$ framework results in structural stability of the PB compound, which gives rise

to a higher capacity and greater cycling stability during the charge-discharge processes. The discharge-charge curves with cycles of the $Na_{1+x}Fe[Fe(CN)_6]$ cathode are plotted in Figure S6. To clearly explore the reason for the greater cycling stability of $Na_{1+x}Fe[Fe(CN)_6]$ cathode, the impedance spectra of $Na_{1+x}Fe[Fe(CN)_6]$ cathode before and after cycles were tested and shown in Figure S7. The impedance curves of $Na_{1+x}Fe[Fe(CN)_6]$ electrodes show two semicircles in the medium frequency and the low frequency regions, which could be assigned to the sodium ion diffusion through the solid electrolyte interphase (SEI) film (R_x) and the charge transfer resistance (R_{ct}), respectively. The R_{ct} is calculated using the equivalent circuit shown in Figure S7(a). The R_{ct} values of the PB-1, PB-3 and PB-5 after 5 cycles are 680 Ω, 468 Ω and 411 Ω, respectively. Clearly, after 30 cycles, the resistance of $Na_{1+x}Fe[Fe(CN)_6]$ electrodes changed a little, suggesting the $Na_{1+x}Fe[Fe(CN)_6]$ framework could maintain a stable structure.

The rate capability of the $Na_{1+x}Fe[Fe(CN)_6]$ cathode was also tested at various current densities from 5 mA g^{-1} (0.05 C) to 100 mA g^{-1} (1 C), as shown in Figure S8. At the current densities of 5, 10, 25, and 100 mA g^{-1}, the PB-5 sample delivered higher capacity than the PB-1 and PB-3 samples. In further work, a composite of the PB-5 sample with carbon can be prepared to improve the rate capability, yielding a cathode which possesses high capacity, stable cycling performance, and high rate capability for sodium ion storage.

CONCLUSION

In summary, Na-enriched $Na_{1+x}Fe[Fe(CN)_6]$ was prepared through a facile and one-step method using $Na_4Fe(CN)_6$ as the precursor in highly concentrated NaCl solutions. With increasing sodium ions entering into the framework, the amount of vacancies and coordinating water in the $Na_{1+x}Fe[Fe(CN)_6]$ decreased, resulting in enhanced structural stability. Thus, the Na-enriched $Na_{1+x}Fe[Fe(CN)_6]$ showed a superior cycling performance with excellent capacity

retention of 97% over 400 cycles. The simple synthesis method, superior cycling stability with a high capacity of more than 100 mAh g^{-1}, and cost-effectiveness make the Na-enriched $Na_{1+x}Fe[Fe(CN)_6]$ a promising cathode for sodium-ion batteries.

METHODS

Synthesis of $Na_{1+x}Fe[Fe(CN)_6]$ cubes

All the chemicals were purchased from Sigma-Aldrich. In a typical procedure, different amounts of NaCl (0, 2, 7, and 21 g, and saturated) were dissolved into 100 mL HCl solutions (0, 0.34, 1.2, 3.6 and 6.16 M, respectively). Then, 581 mg $Na_4Fe(CN)_6 \cdot 10H_2O$ and 1 g poly(vinylpyrrolidone) (PVP, average molar weight of 40,000) were added into the NaCl solutions under magnetic stirring. After vigorous stirring for 1 h, a clear solution was obtained. Vials sealed with caps were placed in an electric oven and heated at 80 $^{\circ}$C for 10 h. The products were collected by centrifugation at 7800 rpm speed for 5 min and washed in distilled water and ethanol several times. After drying, $Na_{1+x}Fe[Fe(CN)_6]$ cubes were obtained. The samples prepared in 0 M, 0.34 M, 1.2 M, 3.6 M and 6.16 M NaCl solutions, are denoted as PB-1, PB-2, PB-3, PB-4, and PB-5, respectively.

Characterization

The crystalline structure of the active powder and electrodes was characterized by powder X-ray diffraction (XRD) on a GBC MMA diffractometer with a Cu K_{α} source. The morphology of the sample was investigated by field emission scanning electron microscopy (FESEM; JEOL JSM-7500FA) and transmission electron microscopy (TEM). X-ray photoelectron spectroscopy (XPS) was conducted using a SPECS PHOIBOS 100 Analyser installed in a high-vacuum chamber with the base pressure below 10^{-8} mbar, and X-ray excitation was provided by Al Kα radiation with photon energy hν = 1486.6 eV at the high voltage of 12 kV and power of 120 W.

Raman spectra were collected using a JOBIN Yvon Horiba Raman spectrometer model HR800, with a 10 mW helium/neon laser at 632.8 nm excitation in the range of 150 to 2000 cm^{-1}. The molar ratios of Na and Fe were measured by inductively coupled plasma (ICP) analysis (Elementar Vario EL CUBE). The amount of water in the samples was determined using a Mettler–Toledo thermogravimetric analysis / differential scanning calorimetry (TGA/DSC) STARe System from 50-600 °C ramped at 10 °C min^{-1} in Ar. ^{57}Fe Mössbauer spectra of the samples were detected at 300 K by using a standard constant-acceleration spectrometer and a ^{57}CoRh source, and the spectrometer was calibrated at room temperature with an α–ion foil. The magnetic measurements were carried out using a 14 T physical properties measurement system (PPMS), equipped with a vibrating sample magnetometer (VSM), over a wide temperature range from 5 K to 300 K in a 100 Oe magnetic field. The phases of PB-1, PB-3 and PB-5 were identified by synchrotron powder X-ray diffraction from the powder diffraction beamline at the Australian Synchrotron, with wavelength of 0.7747Å. In situ synchrotron powder XRD data were collected on the powder diffraction beamline at the Australian Synchrotron with a wavelength (λ) of 0.6888Å, determined using the NIST LaB_6 660b standard reference material. Data were collected continuously in 30 s acquisitions. The cell used for the data collection was charged at a current density of 50 mA g^{-1}, and the cut-off was 2 - 4 V.

Electrochemical test

$Na_{1+x}Fe[Fe(CN)_6]$ electrodes were prepared by mixing 70% active materials, 20% carbon black, and 10% carboxymethyl cellulose (CMC) used as binder by weight to form an electrode slurry, which then was coated on aluminium foil, followed by drying in a vacuum oven overnight at 80 °C, and then pressing with a pressure of 30 MPa. Sodium foil was cut by the doctor blade technique from sodium bulk stored in mineral oil, and it then was employed as both reference

and counter electrode. The electrolyte was 1.0 mol/L $NaClO_4$ in an ethylene carbonate (EC) – diethyl carbonate (DEC) solution (1:1 v/v). The cells were assembled in an argon-filled glove box. The electrochemical performance were tested by a Land Test System in the voltage range of 2–4V (vs. Na^+/Na).

Conflict of Interest: The authors declare no competing financial interest.

Supporting Information. EDS results, SEM images, XPS data, and rate capability of the $Na_{1+x}Fe[Fe(CN)_6]$ are shown in Supporting Information. This material is available free of charge via the Internet at http://pubs.acs.org.

Acknowledgement. This work is supported by the Australian Research Council through a Linkage Project (LP120200432) and Auto CRC 2020, Project 1-111. The authors would like to also thank Dr Tania Silver for critical reading of the manuscript, Dr Dongqi Shi for XPS testing and also acknowledge the use of the facilities in the UOW Electron Microscopy Center, with particular thanks to Dr. Gilberto Casillas-Garcia.

REFERENCES

(1) Yang, Z. G.; Zhang, J. L.; Kintner-Meyer, M. C. W.; Lu, X. C.; Choi, D.; Lemmon, J. P.; Liu, J. *Chem. Rev.* **2011**, 111(5), 3577-3613.

(2) Palomares, V.; Serras, P.; Villaluenga, I.; Hueso, K. B.; Carretero-González, J.; Rojo, T. *Energy Environ. Sci.* **2012,** 5, 5884–5901.

(3) Ong, S. P.; Chevrier, V. L.; Hautier, G.; Jain, A.; Moore, C.; Kim, S.; Ma, X.; Ceder, G. *Energy Environ. Sci.* **2011,** 4, 3680-3688.

(4) Berthelot, R.; Carlier, D.; Delmas, C. *Nature Mater*. **2011,** 10, 74-80.

(5) Yabuuchi, N.; Kajiyama, M.; Iwatate, J.; Nishikawa, H.; Hitomi, S.; Okuyama, R.; Usui, R.; Yamada, Y.; Komaba, S. *Nature Mater*. **2012,** 11, 512-517.

(6) Buchholz, D.; Moretti, A.; Kloepsch, R.; Nowak, S.; Siozios, V.; Winter, M.; Passerini, S. *Chem. Mater*. **2013**, 25, 142-148.

(7) Zhang B.; Liu Y.; Wu X.; Yang Y.; Chang Z.; Wen Z.; Wu Y.; *Chem. Commun*. **2014**, 50, 1209-1211.

(8) Qu Q. T.; Shi Y.; Tian S.; Chen Y. H.; Wu Y. P.; Holze R. *J. Power. Sources*. **2009**, 194, 1222-1225.

(9) Ellis, B. L.; Makahnouk, W. R. M.; Makimura, Y.; Toghill, K.; Nazar, L. F. *Nat. Mater.* **2007**, 6, 749-753.

(10) Liu, Y. L.; Xu, Y. H.; Han, X. G.; Pellegrinelli, C.; Zhu, Y. J.; Zhu, H. L.; Wan, J. Y.; Chung, A. C.; Vaaland, O.; Wang, C. S.; Hu, L. B. *Nano Lett*. **2012**, 12, 5664-5668.

(11) Jian, Z. L.; Han, W. Z.; Lu, X.; Yang, H. X.; Hu, Y. S.; Zhou, J.; Zhou, Z. B.; Li, J. Q.; Chen, W.; Chen, D. F.; Chen, L. Q. *Adv. Energy Mater*. **2013**, 3, 156-160.

(12) Kim, H.; Park, I.; Seo, D. H.; Lee, S.; Kim, S. W.; Kwon, W. J.; Park, Y. U.; Kim, C. S.; Jeon, S.; Kang, K. *J. Am. Chem. Soc*. **2012,** 134, 10369-10372.

(13) Nishijima, M.; Gocheva, I. D.; Okada, S.; Doi, T.; Yamaki, J. I.; Nishida, T. *J. Power. Sources*, **2009,** 190, 558-562.

(14) Wessells, C. D.; Peddada, S. V.; Huggins, R. A.; Cui, Y. *Nano Lett*. **2011**, 11, 5421-5425.

(15) Lu, Y. H.; Wang, L.; Cheng, J. G.; Goodenough, J. B. *Chem. Commun.* **2012,** 48, 6544-6546.

(16) Wang, L.; Lu, Y. H.; Liu, J.; Xu, M. W.; Cheng, J. G.; Zhang, D. W.; Goodenough, J. B. *Angew. Chem., Int. Ed.* **2013**, 52, 1964-1967.

(17) Matsuda, T.; Takachi, M.; Moritomo, Y. *Chem. Commun*. **2013**, 49, 2750-2752.

(18) Wu, X.; Deng, W.; Qian, J.; Cao, Y.; Ai, X.; Yang, H. *J. Mater. Chem. A* **2013,** 1, 10130-10134.

(19) Qian, J.; Zhou, M.; Cao, Y.; Ai, X.; Yang, H. *Adv. Energy Mater.* **2012,** 2, 410-414.

(20) Yu, S. H.; Shokouhimehr, M.; Hyeon, T.; Sung, Y. E. *ECS Electrochem. Lett.* **2013**, 2, A39-41.

(21) Asakura, D.; Okubo, M.; Mizuno, Y.; Kudo, T.; Zhou, H.; Ikedo, K.; Mizokawa, T.; Okazawa, A.; Kojima, N. *J. Phys. Chem. C* **2012**, 116, 8364-8369.

(22) You, Y.; Wu, X. L.; Yin, Y. X; Guo, Y. G. *Energy Environ. Sci.* **2014**, 7, 1643-1647.

(23) Toby, B. H.; Von Dreele, R. B. *J. Appl. Crystal.* **2013**, 46, 544-549.

(24) Vertelman, E. J. M.; Lummen, T. T. A.; Meetsma, A.; Bouwkamp, M. W.; Molnar, G.; Van Loosdrecht, P. H. M.; Van Koningsbruggen, P. J. *Chem. Mater.* **2008**, 20, 1236-1238;

(25) Samain, L.; Grandjean, F.; Long, G. J.; Martinetto, P.; Bordet, P.; Strivay, D. *J. Phys. Chem. C*. **2013**, 117, 9693-9712.

2015

(26) Liu, H.; Strobridge, F. C.; Borkiewicz, O. J.; Wiaderek, K. M.; Chapman, K. W.; Chupas, P. J.; Grey, C. P. *Science*, **2014**, 344, 1252817.

2015

Table of Contents Graphic

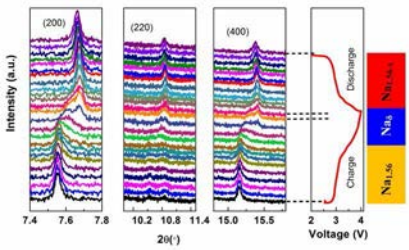

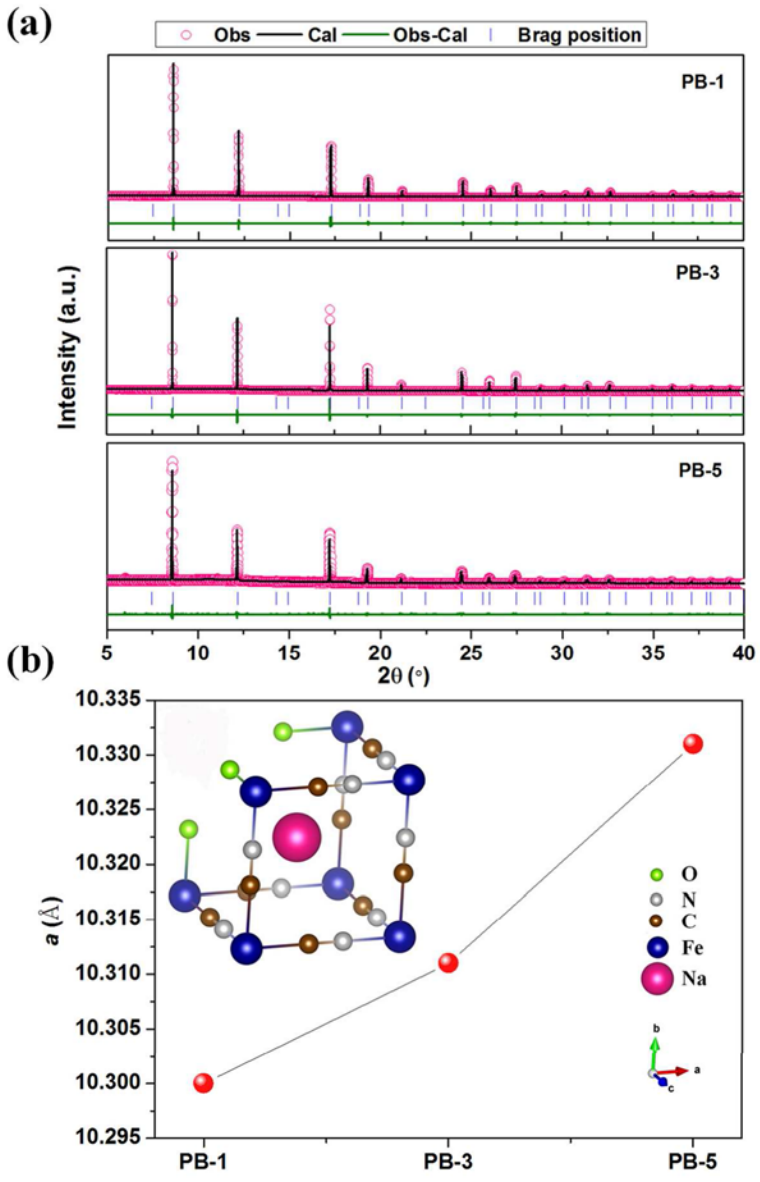

84x128mm (300 x 300 DPI)

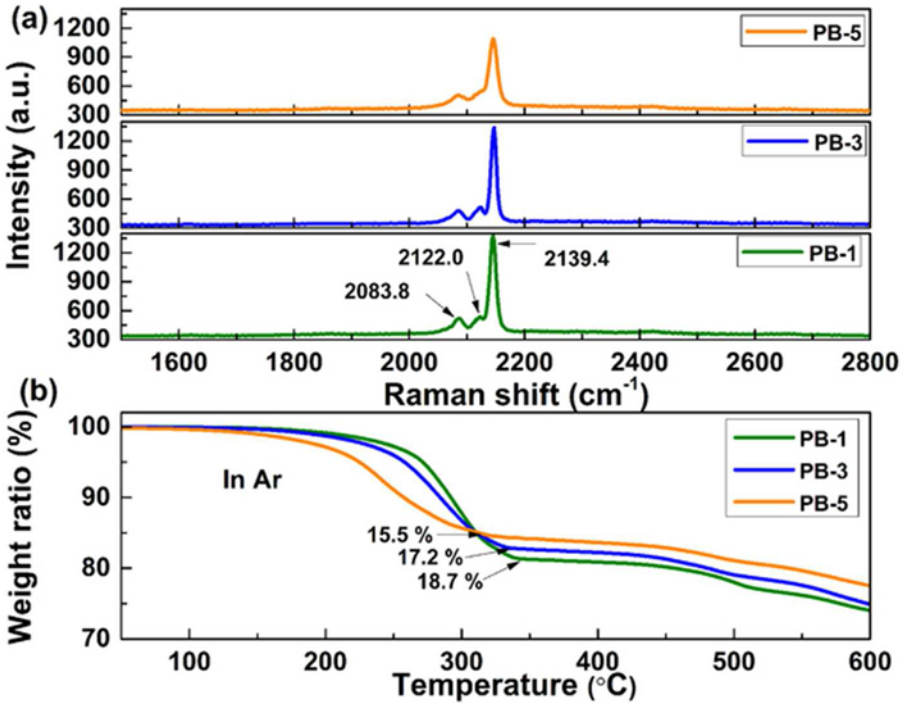

56x39mm (300 x 300 DPI)

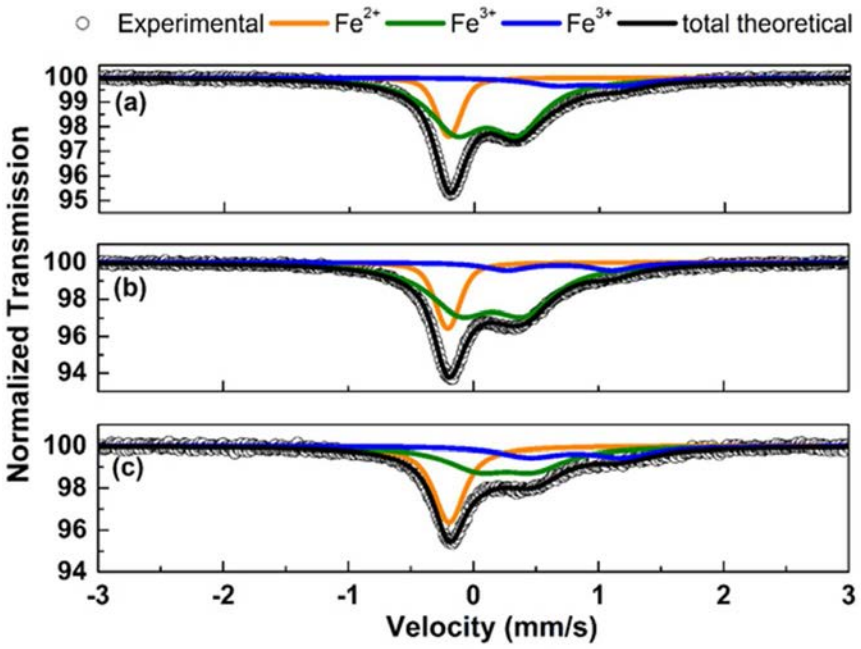

56x39mm (300 x 300 DPI)

2015

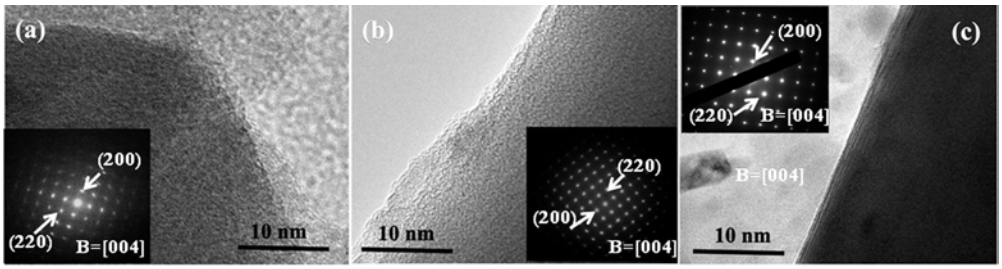

150x39mm (300 x 300 DPI)

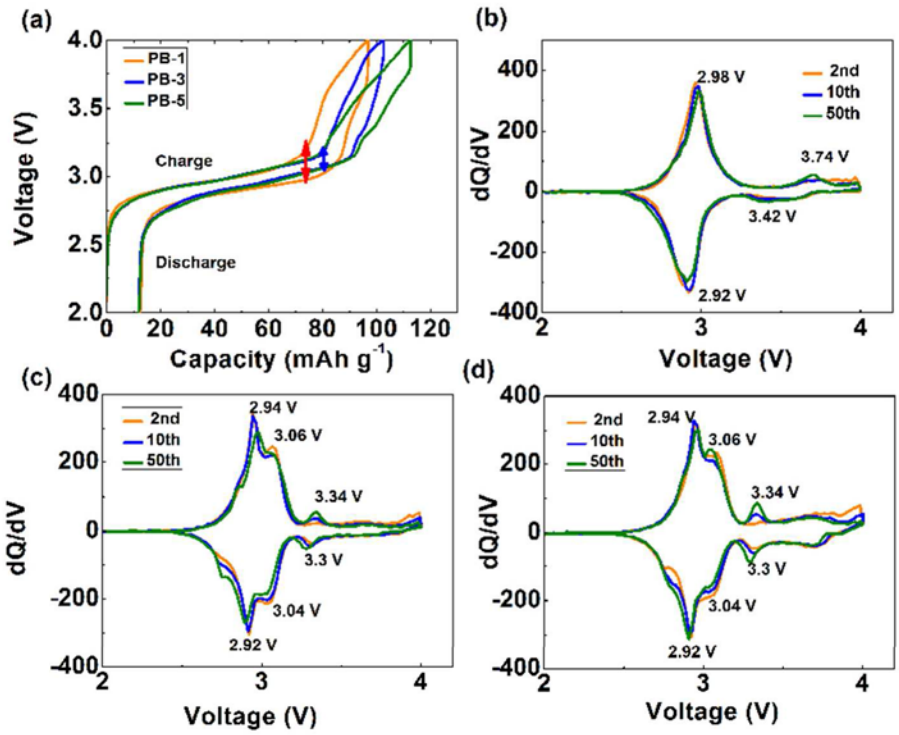

80x62mm (300 x 300 DPI)

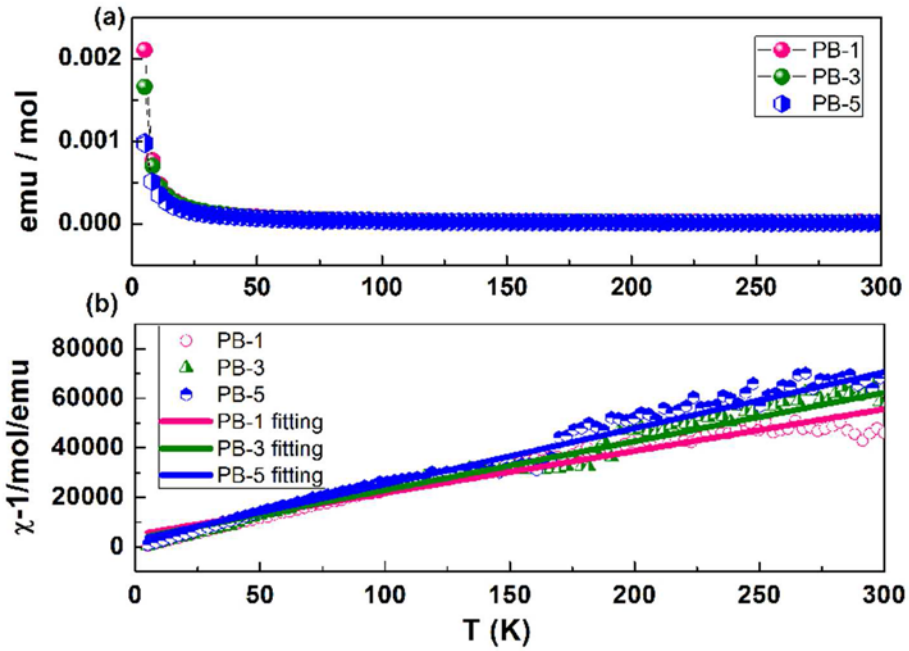

80x56mm (300 x 300 DPI)

2015

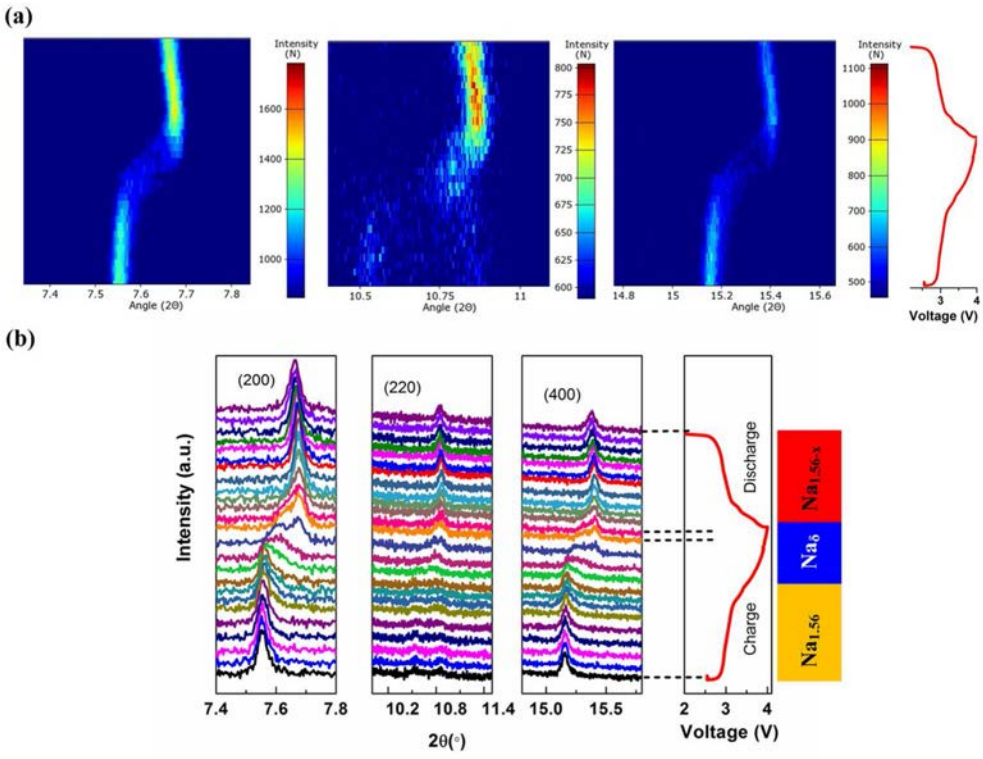

114x87mm (300 x 300 DPI)

2015

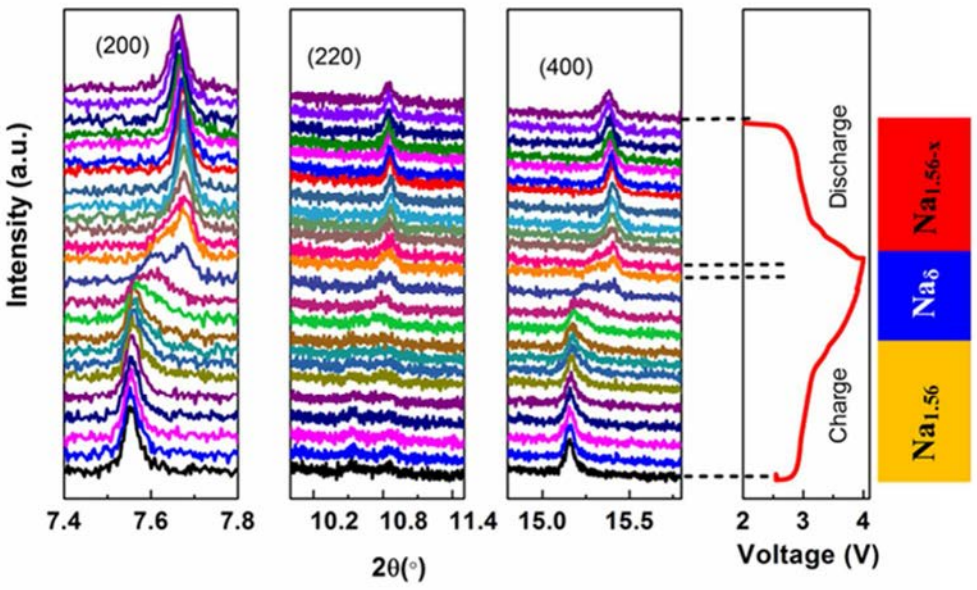

59x35mm (300 x 300 DPI)